Frontiers in Bioscience Landmark

Front. Biosci. (Landmark Ed) **2025**; 30(4): 26654
https://doi.org/10.31083/FBL26654

Original Research

Knockdown of *PAK1IP1* can Induce Pyroptosis to Inhibit the Progression of Hepatocellular Carcinoma

Xiaoliang Lu[1], Jie Chen[1], Zefa Lu[1], Hong Zang[1,*]

[1]Hepatobiliary Surgery Department, Nantong First People's Hospital, 226000 Nantong, Jiangsu, China
*Correspondence: zanghong12_3@163.com (Hong Zang)
Academic Editor: Amancio Carnero Moya
Submitted: 20 September 2024 Revised: 26 December 2024 Accepted: 6 January 2025 Published: 2 April 2025

Abstract

Aim: To identify potential prognostic biomarkers and uncover new mechanisms underlying hepatocellular carcinoma (HCC). **Background:** HCC is a prevalent and fatal malignancy originating from hepatic cells, with a consistently rising incidence in recent decades. Objective: To identify potential prognostic biomarkers, specifically focusing on the role of PAK1-interacting protein 1 (PAK1IP1), and to uncover novel mechanistic insights in HCC. **Methods**: HCC-related datasets (GSE45267 and GSE49515) and data from The Cancer Genome Atlas (TCGA) were retrieved for the analysis of differentially expressed genes (DEGs). The common DEGs were subsequently subjected to weighted gene co-expression network analysis (WGCNA), protein-protein interaction network (PPI), risk model, expression, survival, and prognostic nomogram to determine key genes associated with HCC. Further, the key gene was analyzed using clinical feature analysis, immunoassay, and cell experiments to investigate its exact role in HCC. **Results**: Based on the above comprehensive analysis, we targeted the key gene *PAK1IP1* with a good prognostic value in HCC. *PAK1IP1* showed a remarkably higher increase in tumor samples than in normal samples, which might be related to immune cell infiltration in liver cancer. It was up-regulated in HCC cells, and its knockdown could suppress HCC proliferation and migration. Besides, enzyme-linked immunosorbent assay (ELISA) showed that *PAK1IP1* could regulate lipopolysaccharide (LPS)—induced pyroptosis of HCC cells. Knocking down *PAK1IP1* could lead to increased expression of caspase 3 (CASP-3), gasdermin E (GSDME)-N, cleaved caspase-1, and gasdermin-D (GSDMD)-N in HCC cells, inducing pyroptosis, thereby inhibiting the development of HCC. **Conclusion**: To summarize, *PAK1IP1* was identified as a promising prognostic biomarker, and the knockdown of *PAK1IP1* can induce pyroptosis to suppress HCC development, which sheds new light on HCC tumorigenesis.

Keywords: hepatocellular carcinoma; pyroptosis; *PAK1IP1*; CASP-3; Z-DEVD-FMK; prognostic biomarkers

1. Introduction

Liver cancer, or hepatocellular carcinoma (HCC), is a prevalent and fatal malignancy originating from hepatic cells [1]. Its incidence has shown a consistent rise in recent decades, making it one of the most common malignancies to be diagnosed globally [2]. The current treatment options for HCC encompass surgical intervention, chemotherapy, radiation therapy, targeted therapy, and immunotherapy [3]. The appropriate treatment modality is up to the cancer stage, overall health status, liver function, and other factors [4]. Despite the availability of several therapeutic options, the 5-year survival rate for individuals with HCC is still poor, at about 18%. Thus, developing a reliable prognostic model that integrates clinical, laboratory, and molecular biomarkers is crucial for guiding the clinical management of HCC patients [5]. Prognostic factors commonly employed in HCC encompass clinical parameters, laboratory data, radiological findings, and molecular biomarkers [6]. With the advancement of artificial intelligence and machine learning, numerous studies have focused on constructing predictive models to enhance the accuracy of prognostic predictions, which holds great promise in providing valuable insights for the customized therapy of HCC patients.

Pyroptosis was initially discovered in the 1970s [7]. It is a form of programmed cell death (PCD) characterized by cellular swelling, culminating in cell membrane rupture and the release of cellular contents, thereby inciting a robust inflammatory response [8]. This process of inflammatory cell death, also known as cellular inflammatory necrosis, plays a pivotal role in tumor suppression by stimulating anti-tumor immune responses. Pyroptosis is orchestrated by activating the inflammasome upon sensing endogenous danger signals or environmental stimuli, which recruits and activates caspase (CASP) [9]. Activated caspase has a dual role; it not only cleaves and activates inflammatory factors such as interleukin (IL)-18 and IL-1β but also cleaves Gasdermin-D (GSDMD), inducing cell membrane perforation and triggering cell pyroptosis [10]. In the context of liver cancer, researchers have found that inducing pyroptosis holds significant therapeutic potential for cancer treatment. Several studies have demonstrated that liver cancer cells are more susceptible to pyroptosis induction than normal cells [11,12]. Furthermore, regulating HCC cell death through pyroptosis involves various factors, including the B-cell/CLL lymphoma 2 (Bcl-2) protein family and the tumor suppressor gene *p53* [13]. Pyroptosis is a well-established cellular mechanism of cell death that has

drawn interest from cancer researchers because of its potential applications in cancer therapy [14]. The mechanism and potential uses of copper-dependent pyroptosis in inducing cancer cell death are still under exploration. In liver cancer, inducing pyroptosis shows great promise as a therapeutic approach and ongoing research in this field aims to enhance our understanding of cancer biology, particularly in HCC cells.

In this comprehensive study, we employed a combination of computational and experimental approaches to investigate HCC. Initially, we curated and analyzed datasets from Gene Expression Omnibus (GEO) and the cancer genome atlas (TCGA), utilizing bioinformatics tools to determine key prognostic genes related to HCC. Subsequently, we developed a prognostic risk model and prognostic nomogram to evaluate gene clinical significance. In addition, we employed thorough analyses of clinical features and immune profiles to explore a comprehensive knowledge of these key genes in liver cancer. Subsequently, we conducted cell experiments to investigate the mechanisms by which these key genes, as well as pyroptosis-related genes, regulate the development of HCC. Overall, this research contributed to a new understanding of HCC and offered potential targets for clinical applications, offering promising avenues for improved diagnosis and treatment strategies in the field of HCC.

2 Materials and Methods

2.1 Data Origination

We obtained 371 Liver hepatocellular carcinoma (LIHC) samples and 50 normal samples from TCGA. Additionally, we downloaded two publicly available datasets GSE45267 and GSE49515 from GEO (https://www.ncbi.nlm.nih.gov/geo/). Raw data from TCGA and GEO were preprocessed using the "affy" and "limma" packages in R software. Patients' Clinical information, including age, sex, stage, and survival data, was extracted from the TCGA database (https://portal.gdc.cancer.gov/).

2.2 Weighted Gene Co-Expression Network Analysis (WGCNA)

Differentially expressed genes (DEGs) identification was screened on three datasets: GSE45267, GSE49515 and TCGA. Venn diagrams were used to identify overlapping up-and-down-regulated genes. WGCNA is a powerful bioinformatics tool that can identify groups of highly related genes and their relationship to phenotypic traits. We utilized WGCNA to analyze the overlapping genes to determine key module for the following analysis.

2.3 Functional Enrichment Analysis and Molecular Complex Detection (MCODE) Analysis

Next, Gene Ontology (GO) and Kyoto Encyclopedia of Genes and Genomes (KEGG) analysis were conducted. $p < 0.05$ was used to determine the significance of the enriched results. The co-expression network of essential genes also had major modules that we could locate using the Molecular Complex Detection (MCODE) algorithm. MCODE analysis was carried out using the Cytoscape (version 3.8.0, Institute for Systems Biology, Seattle, WA, USA) program by k-core (2), degree cutoff (2), maximum depth (100), and node score cutoff (0.2). These helped us identify key biological pathways and subnetworks relevant to HCC progression.

2.4 Establishment and Validation of Prognostic Risk Model

Least Absolute Shrinkage and Selection Operator (LASSO) regression analysis was conducted on the 75 node genes screened out by the MCODE algorithm, and the minimum lambda value (lambda. min = 0.0166) was selected in this study. A risk score was determined for each TCGA-HCC tumor sample to create a prognostic risk model. We created scatterplots and heatmaps of gene expression for the risk model and identified 26 significant genes. The TCGA samples were split into high- (n = 185) and low-risk (n = 185) groups according to the average risk score, and the Kaplan-Meier database performed the overall survival (OS) analyses. The risk score formula was as follows: Riskscore = (–0.0199) × *RPA1* + (0.2099) × *WDR12* + (0.0206) × *CDK4* + (0.0147) × *DCAF13* + (0.1308) × *FTSJ3* + (0.3767) × *CPSF3* + (–0.1757) × *RFC1* + (–0.1788) × *RRP1B* + (0.1366) × *RMI1* + (–0.0077) × *POLD3* + (0.1838) × *ASF1A* + (0.1581) × *CPSF2* + (0.0078) × *NUP43* + (0.1364) × *XPOT* + (0.0332) × *CCNF* + (0.1683) × *ESF1* + (0.2319) × *PAK1IP1* + (–0.0111) × *NOL12* + (–0.1896) × *DDX59* + (–0.4887) × *RFC3* + (0.487) × *TTK* + (0.0187) × *RRM2* + (0.0052) × *CEP55* + (0.0855) × *ECT2* + (0.0763) × *FBXO5* + (–0.6687) × *ZWILCH*. Then, using receiver operating characteristic (ROC) analysis, we reported 1-, 3-, and 5-year OS and compared OS curves between subgroups. The capability of the model was evaluated by area under the area under curve (AUC).

2.5 Prognostic Gene Expression and Survival Analysis in TCGA and GEO

First, we obtained gene data from TCGA, GSE45267 and GSE49515 datasets, respectively. Then, univariate Cox regression analysis was employed to determine the most critical prognostic genes. Following the identification of potential prognostic genes, we employed a batch survival analysis to evaluate their collective impact on patient survival. For this purpose, we utilized the Kaplan-Meier estimator, a non-parametric statistic, to estimate the survival function from lifetime data. The patient cohort was divided into high and low-expression groups based on the median expression level of each gene.

2.6 Prognostic Nomogram Construction

The Cox proportional hazards model is a widely applied statistical method for survival analysis, which considers the influence of multiple variables on the survival time of patients. Herein, we applied univariate/multivariate

Cox analyses to investigate the prognostic value of 19 genes with significant expression in survival analysis. Multivariate Cox analysis was used to assess the individual prognostic potential of each gene after adjusting for other covariates. Finally, we selected genes substantially related to survival outcomes in univariate and multivariate Cox analyses to construct prognostic nomograms. The nomogram was further validated using a calibration curve.

2.7 Clinical Feature Analysis of Key Gene and Immune Score Evaluation

In this study, we utilized the University of Alabama at Birmingham Cancer (UALCAN) (http://ualcan.path.uab.edu/index.html) database to study the levels and trends of key genes in the clinical characteristics of liver cancer, including age, gender, individual cancer, TP53 mutation and tumor grade. UALCAN is an interactive portal that provides easy access to TCGA data. The immune scores were then further evaluated using immuneDeconv (version 2.0.2; https://github.com/grst/immunedeconv), which uses gene expression data to evaluate the comparative abundance of immune cell types in tumor samples.

2.8 Cell Culture

American type culture collection (ATCC) provided HCC cell lines (Huh7, Hep3B, HepG2, MHCC97H) and normal liver cells (LO2). HepG2 and MHCC97H were put in RPMI-1640 media with 10% FBS, whereas Huh7 and Hep3B were in Dulbecco's Modified Eagle Medium/Nutrient Mixture F-12 (DMEM/F12) conditions. 10% FBS was added to DMEM to boost the culture of LO2 cells. Experiments were conducted on cells between passages 3 and 8, and cells were subcultured every three to four days. All cell lines were validated by short tandem repeat (STR) profiling and tested negative for mycoplasma.

2.9 Quantitative Reverse Transcription Polymerase Chain Reaction (qRT-PCR)

We conducted siRNA transfection using Lipofectamine RNAiMAX Transfection Reagent (13778150; Thermo Fisher Scientific, Waltham, MA, USA). Total RNA was collected from the cells 48 hours after transfection by TRIzol reagent (15596018; Invitrogen, Carlsbad, CA, USA). Utilizing the StepOnePlus Real-Time PCR System (4376357; Thermo Fisher Scientific, Waltham, MA, USA) and SYBR Green PCR Master Mix (4309155; Thermo Fisher Scientific, Waltham, MA, USA), qRT-PCR analysis was carried out. The primers for *PAK1IP1* were as follows: Forward 5′-AGTTATGCTCAGTTCCAATCCAGT-3′ and Reverse 5′-CAAGGAGGCAGTGTGAGCAT-3′; for GAPDH: Forward 5′-ACAGTCAGCCGCATCTTCTT-3′ and Reverse 5′-GTTAAAAGCAGCCCTGGTGA-3′.

2.10 Western Blotting (WB)

Using RIPA buffer enhanced with protease and phosphatase inhibitors (78430; Thermo Fisher Scientific, Waltham, MA, USA), total protein was recovered from cells. The BCA protein assay kit (23225; Thermo Fisher Scientific, Waltham, MA, USA) was applied to calculate the protein concentration. Electrophoresis was used to separate equal quantities of protein (20–40 µg) put onto 10–12% SDS-PAGE gels. A wet transfer technique was then employed to transfer the isolated proteins onto nitrocellulose or PVDF membranes. Membranes were kept with primary antibodies at 4 °C overnight after being blocked with 3% BSA in TBST for an hour. Primary antibodies include: PAK1IP1 (Cat No. 16071-1-AP, 1:2000; Proteintech, Wuhan, China), gasdermin E (GSDME) (ab215191, 1:1000; Abcam, Shanghai, China), Pro-CASP3 (ab32150, 1:1000, Abcam, Shanghai, China), Cleaved-CASP3 (Cat no. 82707-13-RR, 1:5000; Proteintech, Wuhan, China), GSDMD (Cat No. 20770-1-AP, 1:2000; Proteintech, Wuhan, China), GSDMD-N (FNab10690, 1:1000; Wuhan Fine Biotech Co., Ltd., Wuhan, China), Cleaved-caspase-1 (Cat no. 4199, 1:1000; Cell signaling Technology, Danvers, MA, USA), GAPDH (ab8245, 1:10000; Abcam, Shanghai, China) The membranes were TBST-washed before incubation for an hour with secondary antibodies (ab9482, 1:5000; Abcam, Shanghai, China) that were HRP-conjugated. An excellent chemiluminescent substrate (ECL) substrate was used to see the protein bands, and imaging equipment (Model Gel Doc XR+, Hercules, CA, USA) was used to take pictures of them. To balance the amounts of protein expression, we employed either β-actin or GAPDH as an internal control. With ImageJ (version 1.53; National Institutes of Health, Bethesda, MD, USA), the bands were quantified.

2.11 Cell Counting Kit-8 (CCK-8) Assay

5×10^3 cells were planted in each well in 96-well plates, and the cells were then left to attach for 24 hours. After treatment with the experimental reagents, the CCK-8 solution (CK04; Dojindo Molecular Technologies, Kumamoto, Japan) was diluted to 10 µL in each well, and the plates were incubated at 37 °C for 1–4 hours. The absorbance at 450 nm was measured with a microplate reader (Multiskan™ GO Microplate Spectrophotometer Thermo Scientific, Waltham, MA, USA). By contrasting the absorbance of treated and control cells, the vitality of the cells was determined. The experiments were carried out three times, and the mean standard deviation was used to show the findings.

2.12 Transwell Assay

Cells were put into the upper chamber of a Transwell insert with an 8 µm hole size for the migration test after being suspended in serum-free DMEM. 10% FBS-containing media was put into the bottom chamber. The upper chamber of the Transwell insert had Matrigel (BD Biosciences, San Jose, CA, USA) precoated for use in the invasion experiment. Cells were suspended in serum-free media to seed the upper chamber. 10% FBS-containing media was put

into the bottom chamber. The migrating and invading cells were fixed and stained with DAPI. The amount of invading or migrating cells was counted after microscopically (BX51; Olympus, Tokyo, Japan) captured images.

2.13 Enzyme-Linked Immunosorbent Assay (ELISA) Assay

To assess the amounts of IL-1β protein expression in cell culture supernatants, the enzyme-linked immunosorbent assay (ELISA) was used. At 4 °C, 96-well plates were coated with anti-IL-1β capture antibody (ab9722, 0.5 µg/mL; Abcam, Shanghai, China) overnight. The wells were filled with the cell culture supernatants and cultured for 2 hours indoor after blocking with 1% bovine serum albumin (A7030; Sigma-Aldrich, St. Louis, MO, USA) in Phosphate buffered saline (PBS) for 2 hours. Anti-IL-1β detection antibody that had been biotinylated was then added to the wells and incubated for an additional hour indoor in a solution containing 1% bovine serum albumin and PBS. Streptavidin-horseradish peroxidase (S911, 1:5000 dilution; Thermo Fisher Scientific, Waltham, MA, USA) was added to each well after three PBS washes with 0.05% Tween 20 (P1379; Sigma-Aldrich, St. Louis, MO, USA) were completed. Each well was then kept for 30 minutes. Finally, the wells were rinsed with PBS with 0.05% Tween 20, and the reaction was developed using a tetramethylbenzidine substrate solution (N301; Thermo Fisher Scientific, Waltham, MA, USA). A microplate reader (Multiskan™ GO Microplate Spectrophotometer Thermo Scientific, Waltham, MA, USA) detected the optical density at 450 nm. The content of IL-1β in the cell culture supernatants was computed based on the standard curve. All samples were run in duplicate.

2.14 Statistical Analysis

Various bioinformatics and statistical analysis packages of R language (version 4.1.3; R Foundation for Statistical Computing, Vienna, Austria; https://www.r-project.org/) were employed, such as edgeR (version 3.9; http://bioconductor.org/packages/edgeR/), limma (version 4.1; http://bioconductor.org/packages/limma/), survival (version 3.2.11; http://CRAN.R-project.org/package=survival), ggplot2 (version 3.5.1; https://ggplot2.tidyverse.org/), etc. We preprocessed each dataset, including normalization of gene expression levels and correction for batch effects. For the screening of DEGs, we applied the edgeR and limma packages to screen for differentially expressed genes, and set the significance level as FDR <0.05 and $\log_2$ fold change >1 or <-1. The data were analyzed using a one-way analysis of variance (ANOVA) by the R function "aov" for multiple comparisons and a two-tailed Student's t test for group comparisons. The findings were expressed as mean $\pm$ standard deviation representing the data. We conducted the aforementioned experiments at least three times, and used $p < 0.05$ for the purpose of determining statistical significance.

3. Results

3.1 Identification of DEGs and Key Module in WGCNA

We performed a comprehensive analysis of liver cancer using a multi-database integration. We found 8977 up- and 1001 down-regulated DEGs from the TCGA dataset (Fig. 1A), 4717 up- and 2343 down-regulated DEGs from the GSE45267 dataset (Fig. 1B), and 3442 up and 1682 down-regulated DEGs (Fig. 1C). The Venn diagram revealed 1163 upregulated and 76 downregulated genes at the intersection (Fig. 1D,E). By using WGCNA analysis, we determined a soft threshold power of 1 (Fig. 1F). Two modules were identified based on the clustering dendrogram (Fig. 1G) and measured the relation between module eigengenes (ME) and clinical characteristics; the turquoise module was the key module for subsequent analysis (Fig. 1H).

3.2 The Functional Enrichment Analysis and PPI Networks of the Turquoise Module

The genes in the turquoise module were related to the DNA metabolic process, Mitotic spindle organization, and DNA repair (Fig. 2A). Furthermore, enriched pathways included RNA transport, Herpes simplex virus 1 infection, Cell cycle, and DNA replication (Fig. 2B). Additionally, we utilized the MCODE algorithm to analyze the protein-protein interaction (PPI) network of the turquoise module genes. Fig. 2C,D present the PPI networks of the turquoise module genes, highlighting two significant clusters, MCODE Cluster 1 and MCODE Cluster 2, with 30 and 45 nodes and 379 and 247 edges, respectively. These clusters indicate densely interconnected groups of genes within the turquoise module, suggesting their involvement in significant biological pathways or processes crucial to HCC tumorigenesis. The nodes symbolize individual genes, and the edges denote their interactions, with larger nodes reflecting higher connectivity. The distinct structures of these clusters may imply different sub-pathways or mechanisms within HCC-related biological processes, potentially linked to tumor progression or treatment resistance. These figures collectively underscore the complex interplay among the genes in the turquoise module and their probable role in HCC development.

3.3 Identification of Prognostic Genes through Construction of Risk Model for HCC

Fig. 3A–C collectively illustrate the process of developing a prognostic risk model and the identification of key genes that can predict survival outcomes in liver cancer. Fig. 3A presents the LASSO regression analysis on nodal genes, showing the distribution of coefficients across a range of lambda values, which is a tuning parameter that controls the regularization strength (Fig. 3A). Fig. 3B identifies the optimal lambda.min value through cross-validation, which is 0.0166, minimizing the mean cross-validated prediction error (Fig. 3B). Fig. 3C depicts the risk score distribution and gene expression levels for the 26 prognostic genes, indicating a correlation between

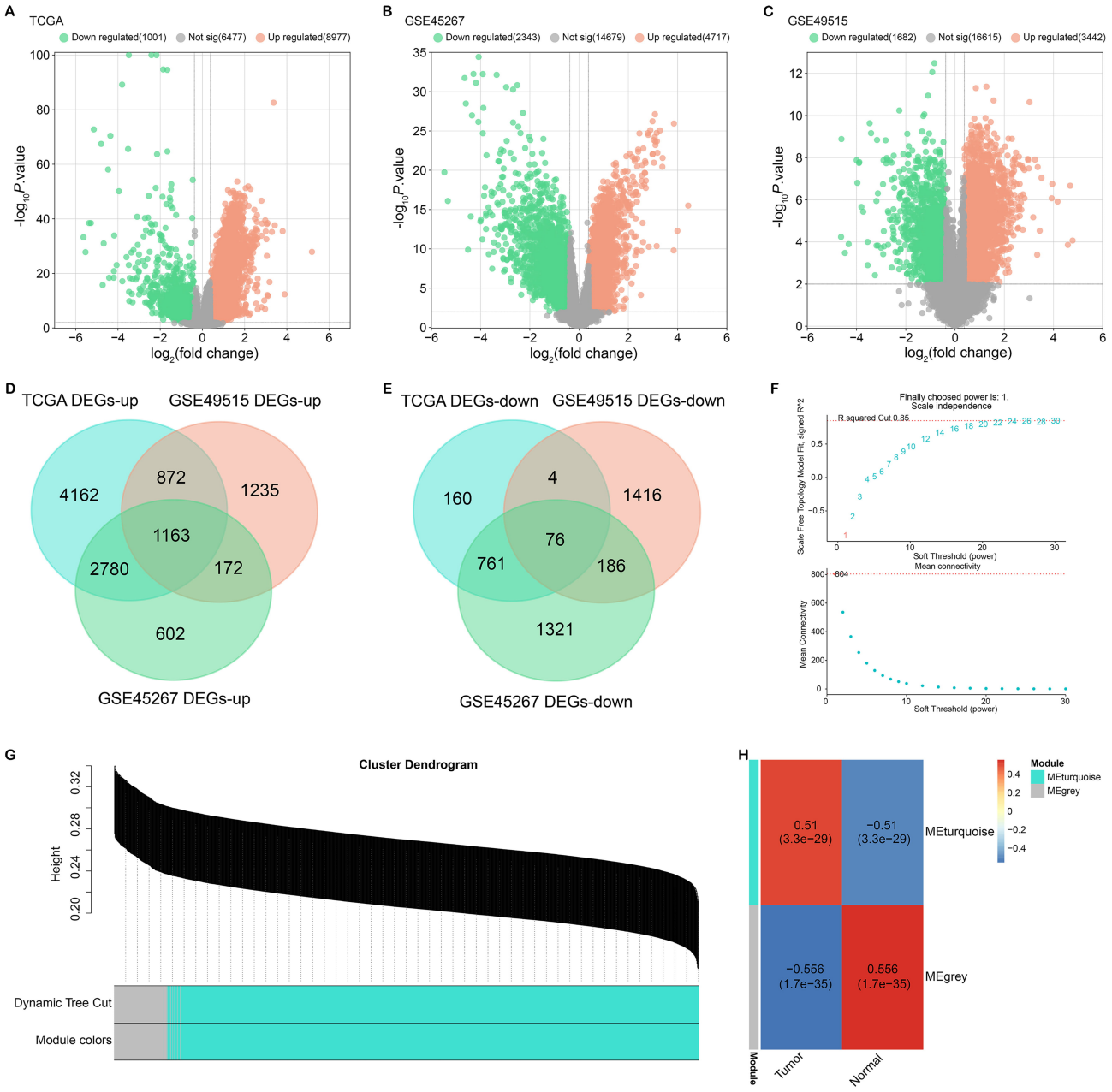

Fig. 1. Identification and WGCNA analysis of DEGs in liver cancer. (A–C) Volcano plots showing identified DEGs from the TCGA dataset (A), GSE45267 dataset (B) and GSE49515 dataset (C). Orange and green dots represent up-regulated and down-regulated genes, respectively. (D) Venn diagram showing the intersection of upregulated DEGs from the three datasets. (E) Venn diagram showing the intersection of downregulated DEGs from the three datasets. (F) Determination of soft threshold power using WGCNA analysis. (G) Dendrogram of gene clustering in WGCNA analysis, with modules indicated by color. (H) Correlation heatmap showing correlations between modular eigengenes (MEs) and clinical features. The Turquoise module was identified as a key module related to clinical features. WGCNA, weighted gene co-expression network analysis; DEGs, differentially expressed genes.

gene expression (z-scores) and patient survival status, with higher risk scores being associated with higher mortality rates. The selection of these 26 genes is based on their statistical significance and strong association with patient survival, as determined by the LASSO regression analysis, aiming to provide a more accurate risk assessment for liver cancer patients. In addition, the OS analysis revealed the high-risk group's survival prognosis was poorer (Fig. 3D). Besides, ROC analysis showed AUC values of 0.858, 0.79, and 0.749 for the first, third, and fifth years, respectively (Fig. 3E). These findings provided valuable insights into HCC prognosis and highlighted the potential clinical utility of the identified prognostic genes and risk models.

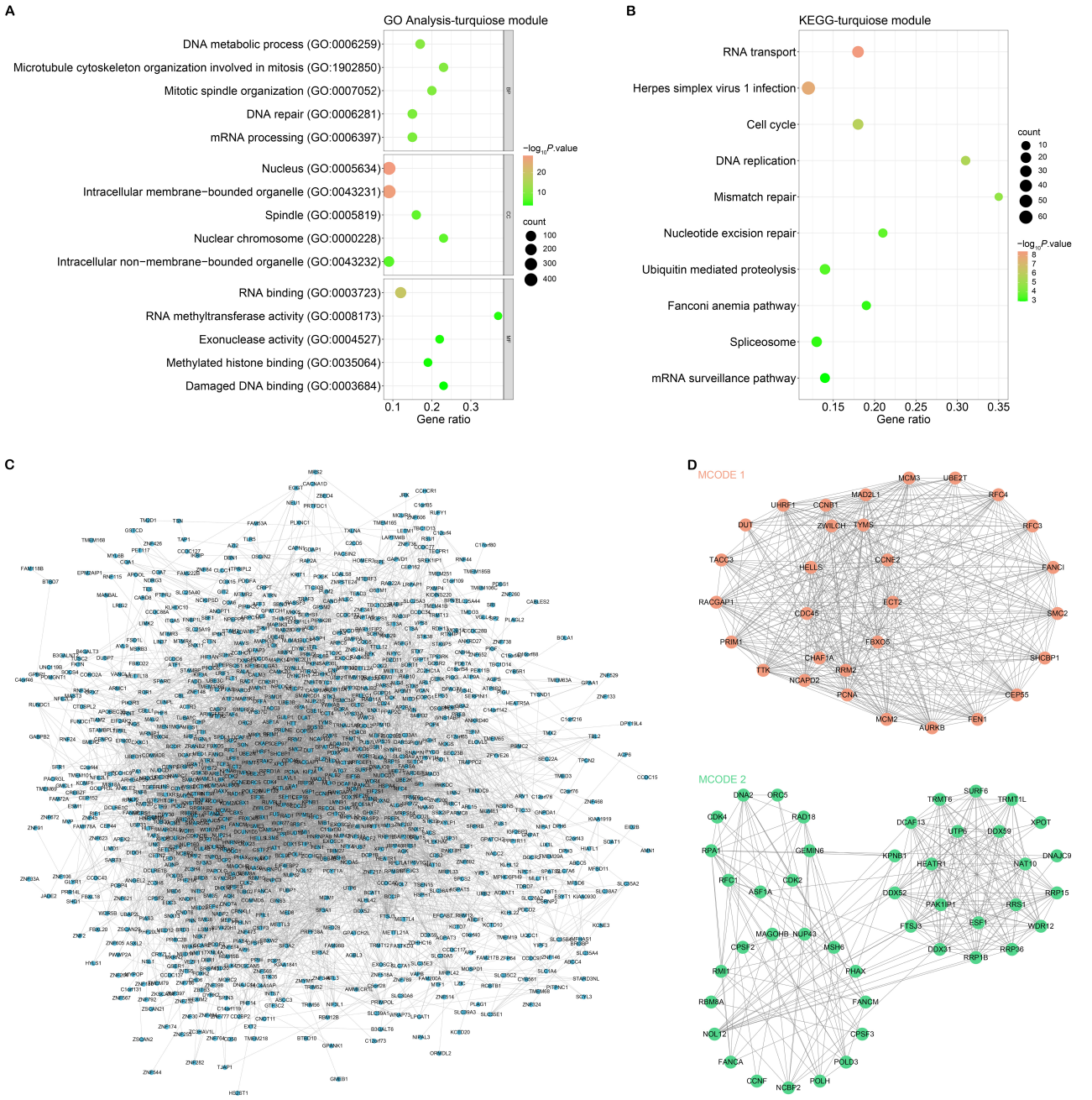

Fig. 2. GO, KEGG pathway enrichment analysis and MCODE networks of turquoise module genes. (A) GO analysis of turquoise module gene enrichment. The abscissa is the Gene ratio, and the ordinate is the enriched term. (B) KEGG pathway enrichment analysis of turquoise module genes. The abscissa is the Gene ratio, and the ordinate is the enriched pathway. (C) PPI network of turquoise module genes. (D) PPI network of MCODE 1 cluster (orange nodes) and MCODE 2 cluster (green nodes) in turquoise module genes. Nodes in the network represent genes and edges represent protein-protein interactions. The size of the nodes reflects the degree of connectivity of the corresponding genes. GO, gene ontology; KEGG, Kyoto Encyclopedia of Genes and Genomes; MCODE, molecular complex detection; PPI, protein-protein interaction.

3.4 19 Prognostic Genes Associated With Survival in HCC Patients

We investigated the expressions of 26 prognostic genes in TCGA, GSE45267, and GSE49515 datasets (Fig. 4A–C). Our results demonstrated these genes were up-regulated in tumor samples. Kaplan-Meier survival analysis indicated that 19 genes were significantly linked to poor prognosis, and high expressions demonstrated lower survival (Fig. 4D–V). Together, these 19 genes have potential as prognostic biomarkers for cancer patients and can be used to develop personalized treatment strategies.

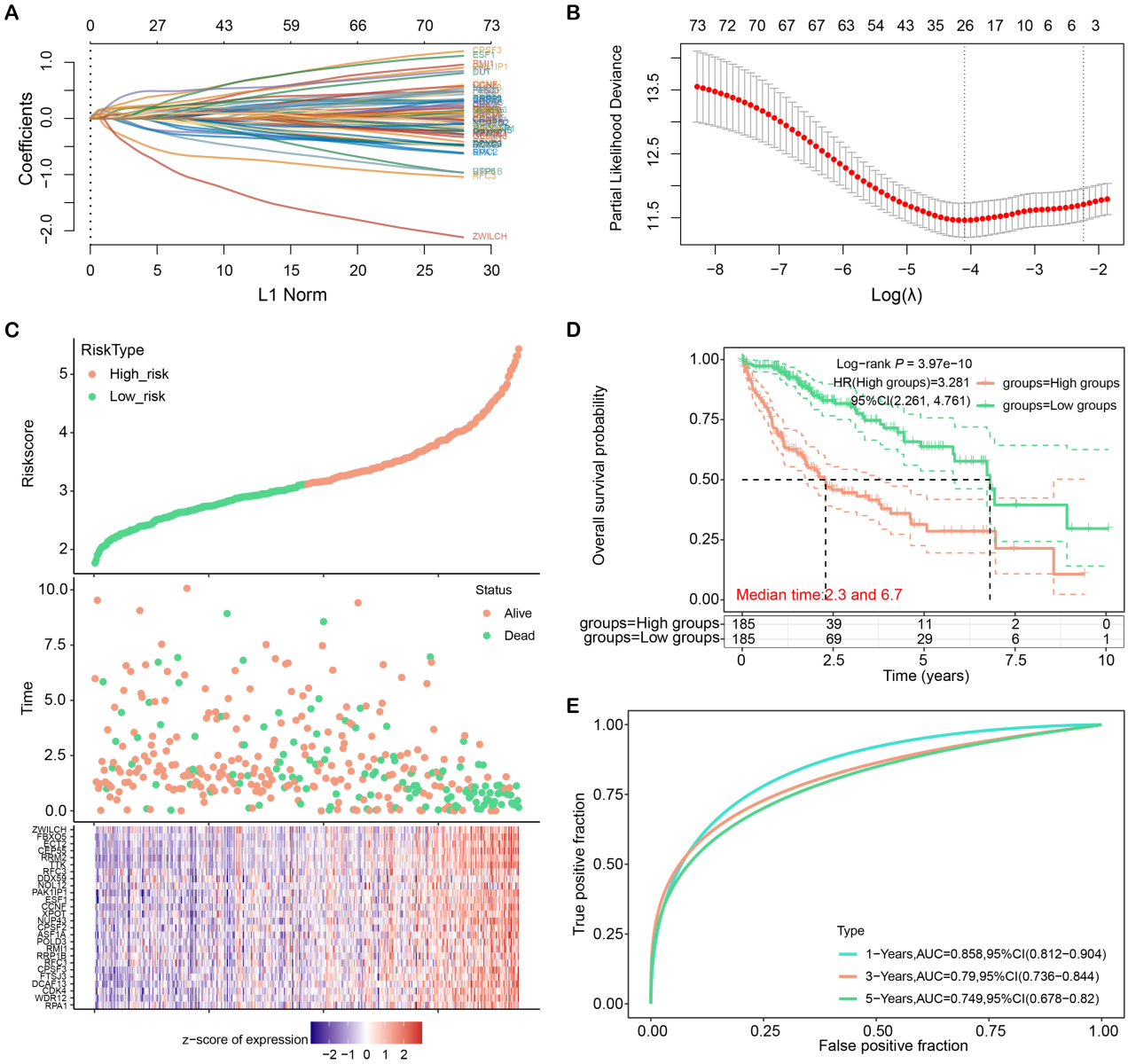

Fig. 3. LASSO regression analysis and construction of liver cancer risk model. (A) Distribution plot of LASSO coefficients for nodal genes. (B) Optimal lambda. min value selected by 10-fold cross-validation. (C) Patient characteristics ordered by their risk score. From top to bottom are the risk scores of 26 genes, the distribution of patient survival status, and the heat map of patients in the low-risk group and high-risk group. (D) Kaplan-Meier curves of overall survival in high-risk and low-risk groups. (E) ROC curves of the liver cancer risk model at 1, 3, and 5 years. ROC, receiver operating characteristic; CI, confidence interval; AUC, area under the curve; LASSO, least absolute shrinkage and selection operator.

3.5 PAK1IP1 is an Individual Prognostic Gene for HCC Patients

In this study, we utilized univariate and multivariate Cox regression analysis to discover that *PAK1IP1* and pathological Tumor-Node-Metastasis (pTNM) stage were individual predictive variables for HCC (Fig. 5A,B). Subsequently, we developed a nomogram by integrating *PAK1IP1* and pTNM stage to enhance the precision of prognosis prediction for HCC patients (Fig. 5C). The calibration plot demonstrated a strong concordance between the projected and observed survival rates (Fig. 5D). These emphasized the value of these two factors in HCC prognosis and the potential of integrating them in a nomogram for clinical use.

3.6 PAK1IP1 Expression Correlates With Immune Cell Infiltration in HCC

Next, we studied the level and clinical significance of *PAK1IP1* in LIHC. According to data from the UALCAN database, *PAK1IP1* level was considerably greater in tumor samples (Fig. 6A). Furthermore, *PAK1IP1* level was higher in HCC patients with older age, male gender, and TP53 mu-

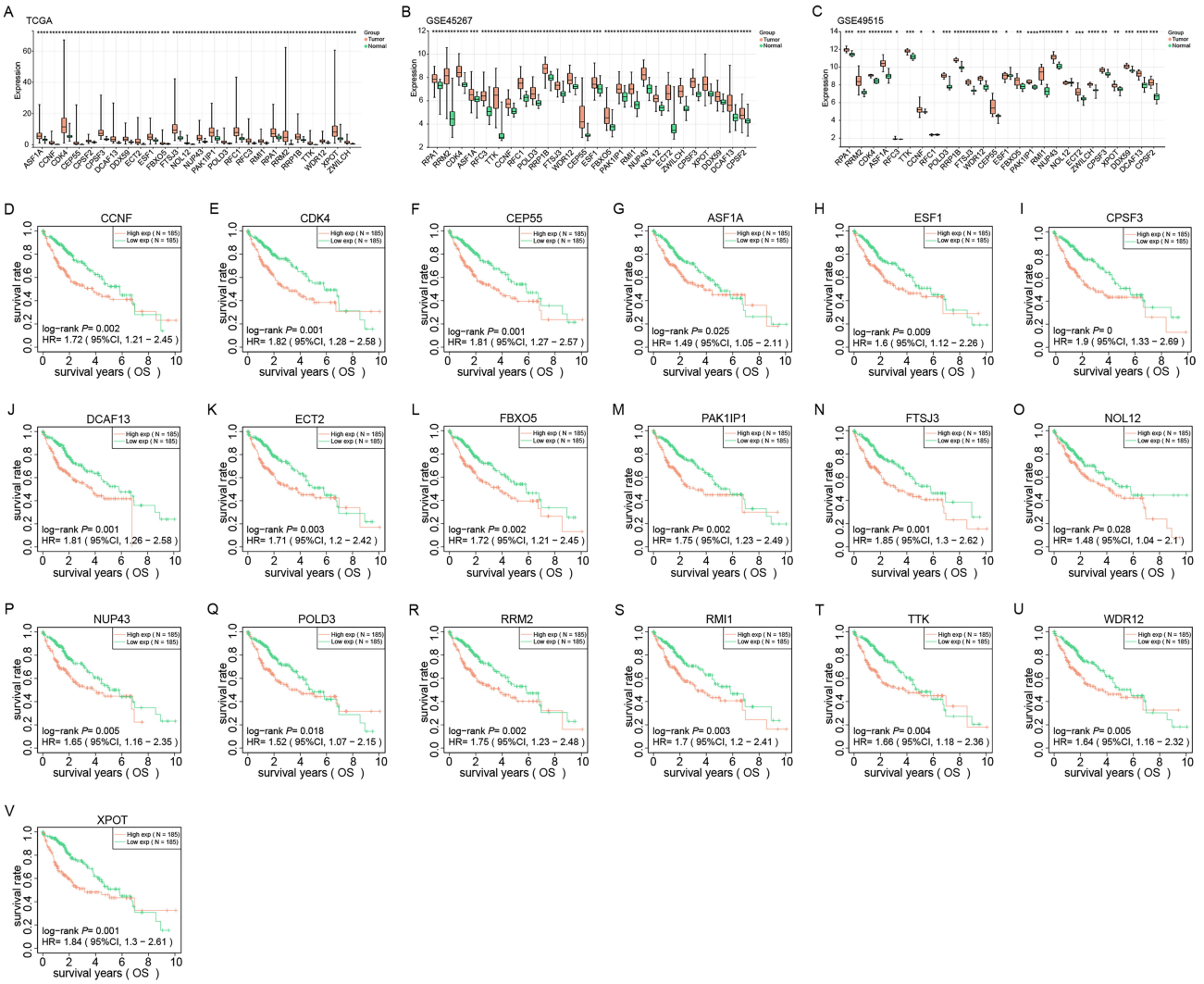

Fig. 4. Expression and prognostic analysis of 26 identified genes in liver cancer. (A–C) Expression levels of 26 genes from TCGA, GSE45267 and GSE49515 datasets in normal and tumor tissues. Red and green represent tumor and normal samples, respectively. (D–V) Kaplan-Meier survival analysis of 19 genes in HCC patients in the TCGA dataset. The X-axis represents the survival time, and the Y-axis represents the survival rate. Red and green curves represent high and low expression groups, respectively. *p*-values and hazard ratios (HR) with 95% confidence intervals (CI) are shown. $*p < 0.05$, $**p < 0.01$, $***p < 0.001$, $****p < 0.0001$. HCC, hepatocellular carcinoma.

tation (Fig. 6B,C,E). In addition, as tumor stage and grade increased, *PAK1IP1* expression also increased (Fig. 6D,F). Next, we identified most immune cells were downregulated in the low *PAK1IP1* expression group, and Myeloid dendritic cells had the highest infiltration percentage in tumor samples (Fig. 6G,H). Our findings suggested that *PAK1IP1* may be a predictive biomarker and be connected to immune cell infiltration.

3.7 PAK1IP1 is Up-Regulated in HCC Cells

We discovered through qRT-PCR analysis that HCC cells (especially Hep3B and HepG2) have higher levels of *PAK1IP1* expression than normal liver cells (Fig. 7A). Our results demonstrated that si-*PAK1IP1*#1 and si-*PAK1IP1*#2 more efficiently reduce *PAK1IP1* expression in HCC cells (Fig. 7B). Moreover, western blotting analysis validated the efficacy of si-*PAK1IP1*#1 and si-*PAK1IP1*#2 in significantly downregulating PAK1IP1 protein levels in HCC cells (Fig. 7C). We then applied CCK-8 assays to assess the impact of *PAK1IP1* knockdown on the proliferation of HCC cells. As expected, *PAK1IP1* knockdown inhibited HCC cell growth (Fig. 7D,E). Additionally, Transwell assays demonstrated that *PAK1IP1* knockdown markedly impeded the invasive and migratory capabilities of HCC cells (Fig. 7F–I).

3.8 PAK1IP1 Knockdown could Activate Lipopolysaccharide (LPS)-Induced Pyroptosis

We constructed a physical interaction network linking *PAK1IP1* and 33 pyroptosis-related genes, as identified in a prior study [15] (Fig. 8A). To investigate whether *PAK1IP1*

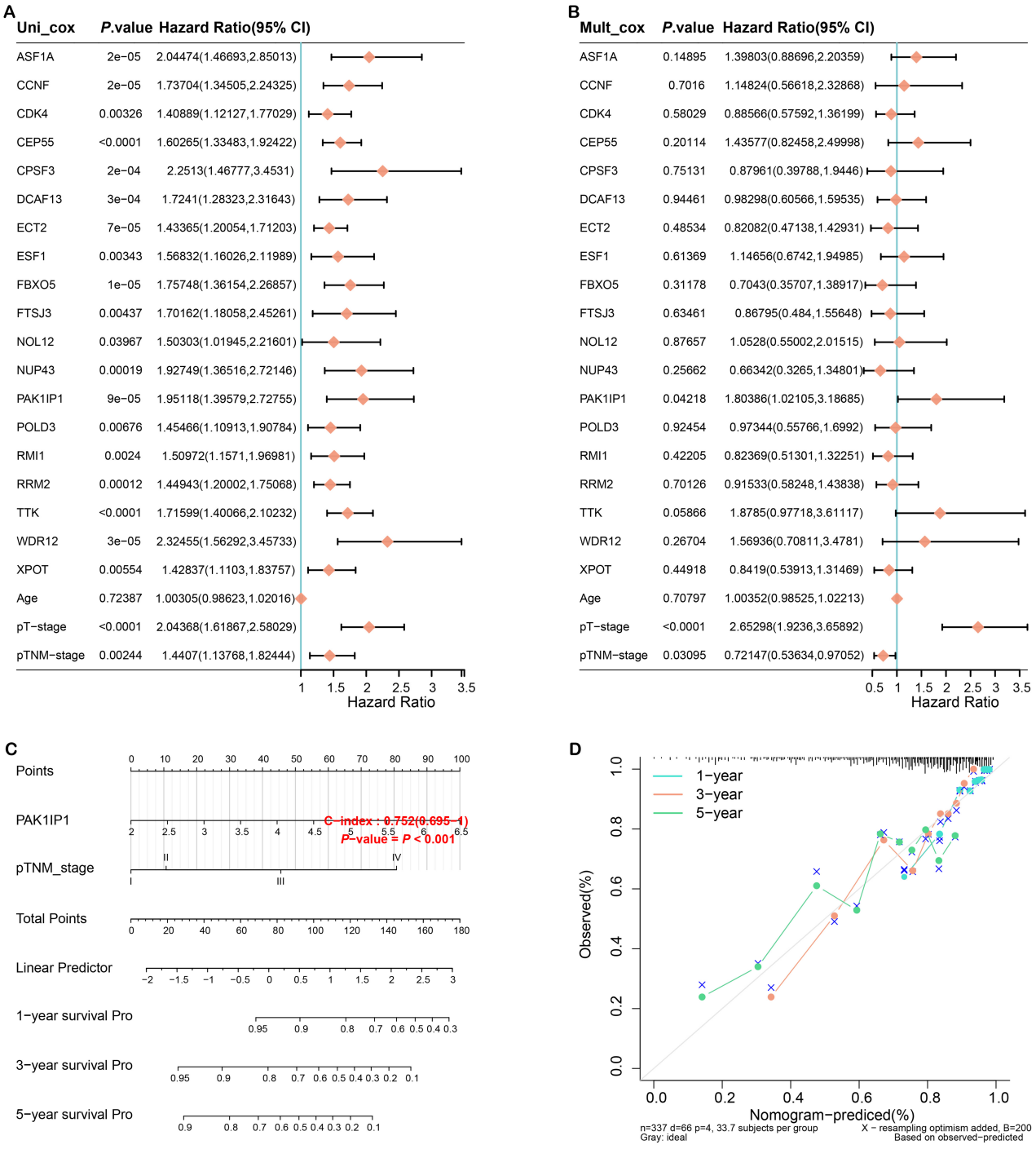

Fig. 5. Construction of the prognostic nomogram. (A) Forest plot of univariate Cox regression analysis of PAK1 interacting protein 1 (*PAK1IP1*) and clinicopathological variables. (B) Forest plot of multivariate Cox regression analysis of *PAK1IP1* and clinicopathological variables. (C) Nomogram for HCC prognosis prediction constructed by integrating *PAK1IP1* and pTNM staging. (D) The calibration plot of the nomogram shows the agreement between predicted and observed survival. The x-axis represents predicted survival probabilities and the y-axis represents actual survival probabilities. Diagonal lines represent perfect predictions. HCC, hepatocellular carcinoma; pTNM, pathological Tumor-Node-Metastasis; 95% CI, 95% confidence interval; pT, pathological tumor; Uni, univariate; Muit, multivariate; Pro, probability.

was related to the regulation of pyroptosis, we measured the production of IL-1β, a quintessential marker of pyroptosis, in HCC cells post-LPS stimulation and subsequent *PAK1IP1* knockdown by ELISA. According to our findings, IL-1 levels considerably increased following LPS treatment and *PAK1IP1* knockdown (Fig. 8B,C).

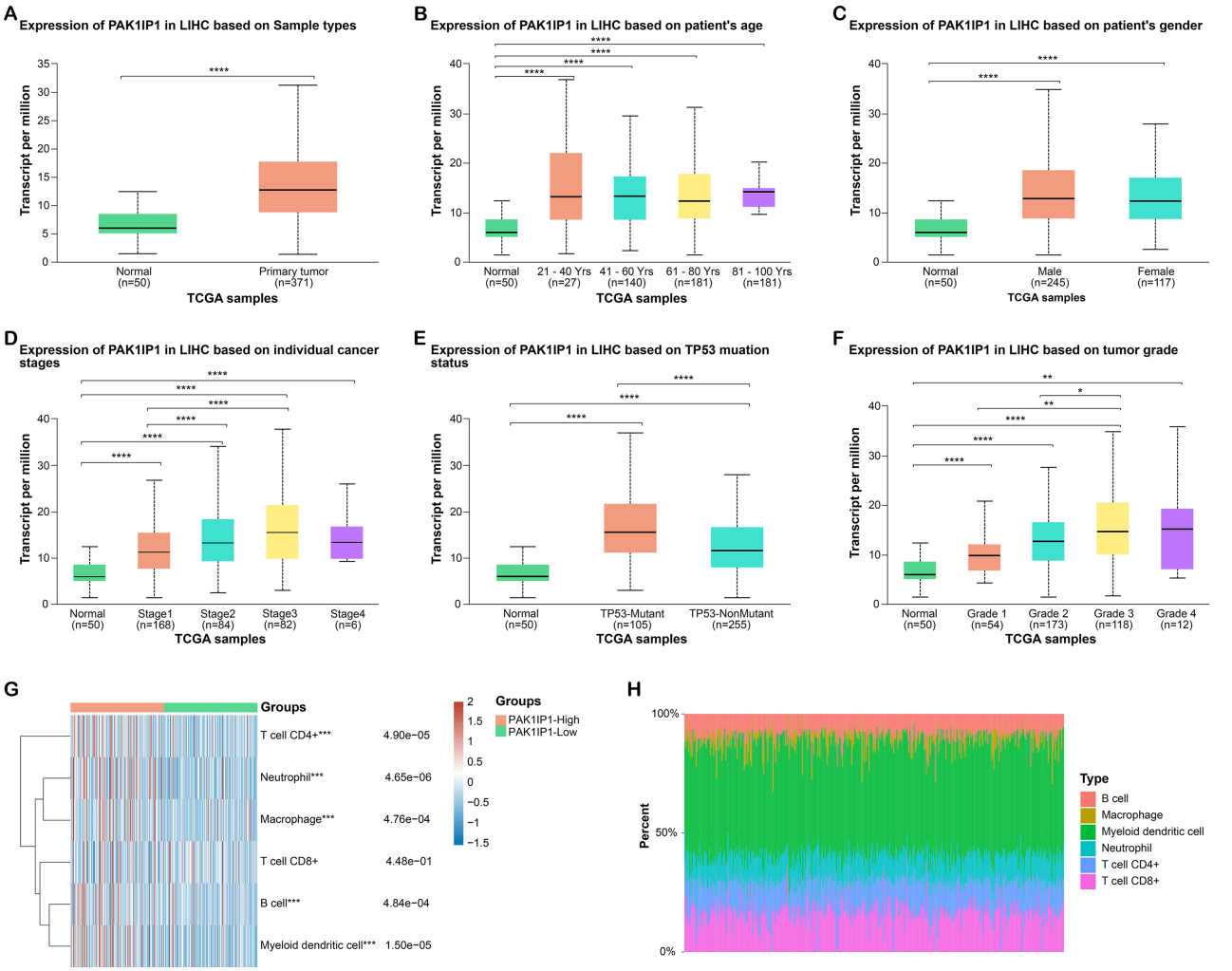

Fig. 6. Clinical feature and immune analysis of *PAK1IP1* in liver cancer. (A) *PAK1IP1* expression levels in normal and tumor samples according to the UALCAN database. (B–F) Boxplot displaying *PAK1IP1* expression levels in individuals with liver cancer, stratified by (B) age, (C) sex, (D) tumor stage, (E) TP53 mutation status, and (F) tumor grade. (G) Heat map of immune cell scores, where different colors represent expression trends in different samples. (H) The percentage abundance of tumor-infiltrating immune cells in each sample. Different colors represent different immune cell types, the abscissa represents the sample, and the ordinate represents the percentage of immune cell content in a single sample. *$p < 0.05$, **$p < 0.01$, ***$p < 0.001$, ****$p < 0.0001$. Yrs, yeras; LIHC, liver hepatocellular carcinoma.

3.9 PAK1IP1 Promotes HCC Proliferation, Invasion and Migration by Inhibiting Pyroptosis

Moreover, we found that *PAK1IP1* inhibition significantly increased the protein levels of CASP-3, GSDME-N, cleaved caspase-1, and GSDMD-N, as detected by WB (Fig. 9A). We subsequently assessed the effects of si-*PAK1IP1* #1 and N-benzyloxycarbonyl-Asp (OMe)-Glu (OMe)-Val-Asp (OMe)-fluoromethyl-ketone (Z-DEVD-FMK) treatment, a CASP-3 inhibitor, on the proliferation of liver cancer cells. The data showed that *PAK1IP1* knockdown significantly reduced HCC cell proliferation, while treatment with Z-DEVD-FMK increased cell proliferation (Fig. 9B,C). Transwell assays further revealed that *PAK1IP1* knockdown suppressed liver cancer cell invasion and migration after LPS treatment, while Z-DEVD-FMK treatment promoted cellular invasion and migration (Fig. 9D–G). These findings indicate that *PAK1IP1* promotes the proliferation, migration, and invasion of HCC cells by inhibiting pyroptosis.

4. Discussion

Biomarkers are a crucial part in the diagnosis, therapy, and prognosis of cancer [16]. Currently, the diagnosis of liver cancer heavily relies on Computed Tomography (CT), Magnetic Resonance Imaging (MRI), and others [17,18]. However, these methods have limitations in detecting early-stage tumors. To address this challenge, targeted gene therapy has become a new therapy for HCC [19]. Nevertheless, its efficiency is hindered by tumor heterogeneity and the development of acquired resistance [20]. Furthermore, the five-year survival rate for liver cancer remains low because

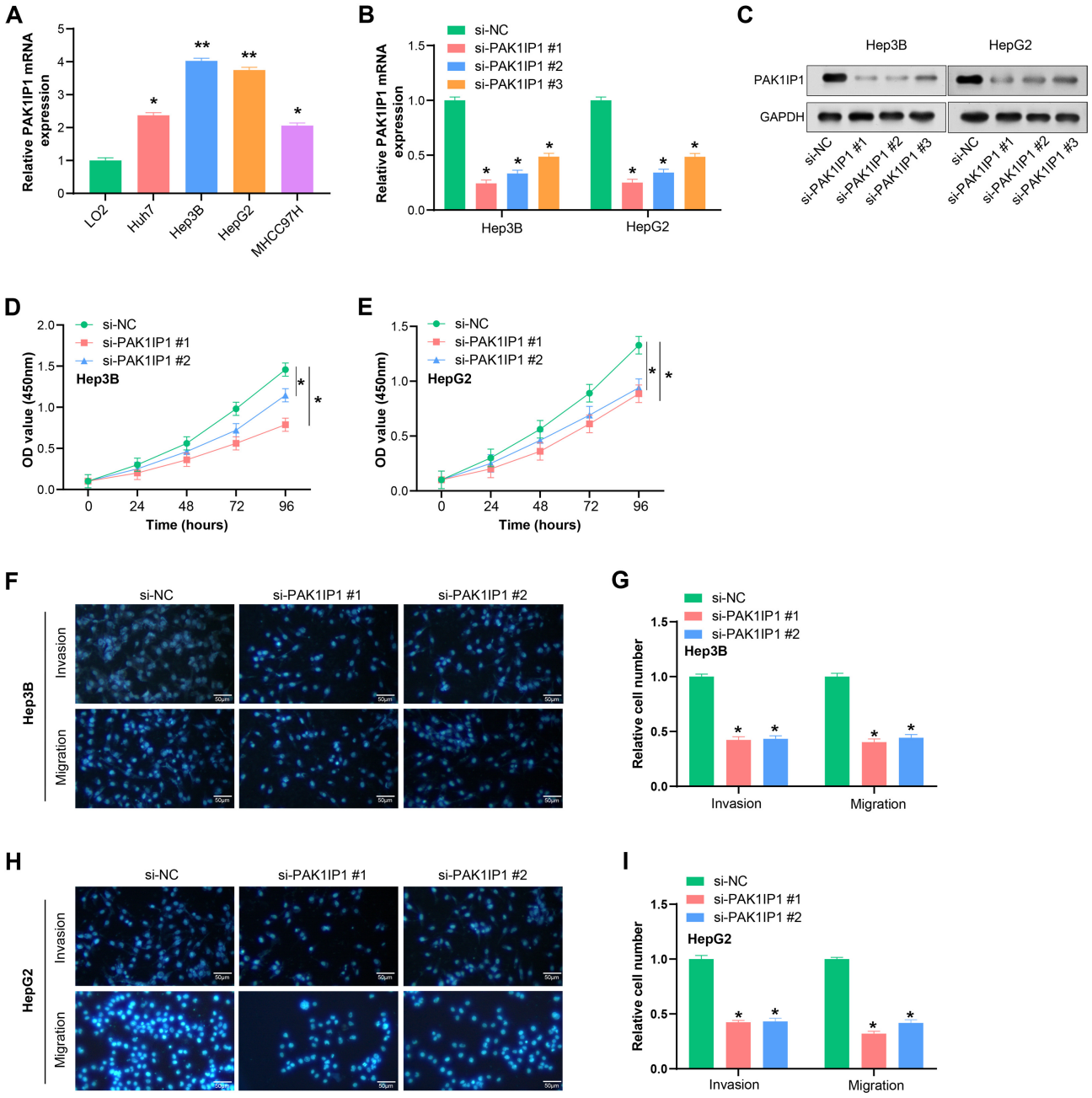

Fig. 7. Knockdown of *PAK1IP1* inhibits growth, invasion and migration of HCC cells. (A) qRT-PCR analysis of *PAK1IP1* expression in normal hepatocytes and HCC cells. (B,C) Efficiency of si-*PAK1IP1* #1, #2 and #3 in HCC cells detected by qRT-PCR and WB in HCC cells. GAPDH was used as a loading control. (D,E) CCK-8 assay showed the effect of *PAK1IP1* knockdown on the proliferation of HCC cells. (F–I) Transwell assay for the effect of *PAK1IP1* knockdown on the invasion and migration of HCC cells. Scale: 50 µm. $*p < 0.05$, $**p < 0.01$. HCC, hepatocellular carcinoma; qRT-PCR, quantitative real-time polymerase chain reaction; WB, western blot; CCK-8, cell counting kit-8; si-NC, small interfering RNA negative control.

of high recurrence and metastasis. Consequently, exploring new efficient biomarkers for the detection, management, and prognosis of liver cancer is urgently needed. These biomarkers could facilitate early detection, guide personalized treatment strategies, and predict patient outcomes. Ultimately, identifying such biomarkers would significantly improve the survival of HCC patients.

Our study identified the turquoise module as an important module associated with liver cancer. The genes in the turquoise module were primarily related to DNA metabolic processes, mRNA processing, nuclear chromosome function, RNA methyltransferase activity, methylated histone binding, Fanconi Anemia pathway, and mRNA Surveillance pathway. These enriched pathways and terms have been extensively studied in HCC and have shown promis-

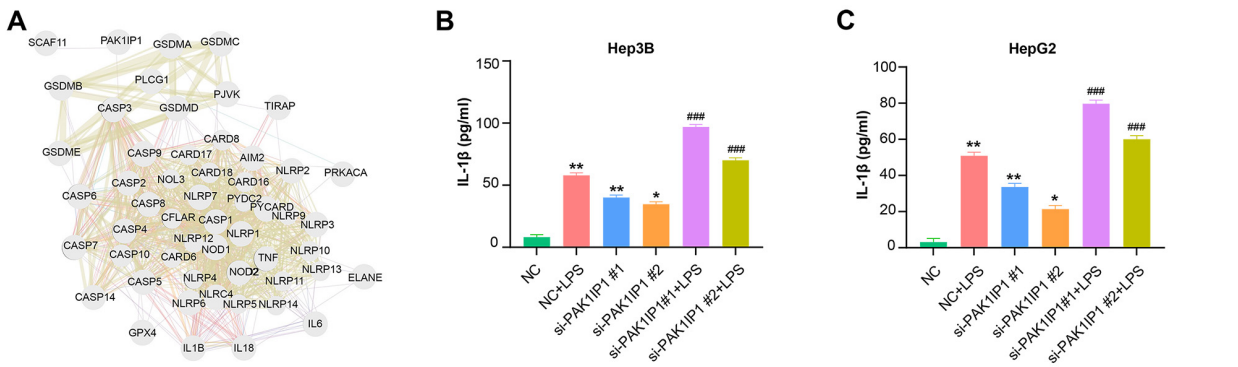

Fig. 8. *PAK1IP1* regulates gene expression associated with pyroptosis in HCC cells. (A) Physical interaction network between *PAK1IP1* and 33 pyroptosis-related genes. Nodes represent genes, and edges represent connectivity between genes. (B,C) ELISA assay to detect the effect of LPS treatment and knockdown of *PAK1IP1* hepatocellular carcinoma cells on pyroptosis-related markers (IL-1β). *$p < 0.05$, **$p < 0.01$. ###$p < 0.001$ vs. si-*PAK1IP1*#1/2. HCC, hepatocellular carcinoma; ELISA, enzyme-linked immunosorbent assay; LPS, lipopolysaccharide; IL, interleukin; NC, negative control.

ing results in improving our understanding of the disease. One of the pathways enriched in the turquoise module is the DNA metabolic process, which plays a crucial role in DNA replication, recombination, and repair [21]. Dysregulation of this pathway has been linked to various cancers, including liver cancer [22]. For example, a study found that the DNA polymerase kappa (POLK) gene's expression in DNA metabolism was upregulated in liver cancer tissues [23]. Another enriched pathway in the turquoise module is the cell cycle. A study reported that compared to nearby normal tissues, the cell cycle pathway gene cyclin dependent kinase inhibitor 2A (*CDKN2A*) was considerably downregulated in liver cancer tissues [24]. Furthermore, low *CDKN2A* level is linked with a poor prognosis in HCC patients [25]. The mismatch repair pathway, involved in correcting errors during DNA replication, is also enriched in the turquoise module. Defects in this pathway have been related to the progression of various cancers. For instance, a study reported that the MutS homolog 2 (*MSH2*) gene's expression in the mismatch repair pathway was downregulated in liver cancer tissues [26]. Moreover, our 26-gene risk model offers several distinct advantages over existing models. Firstly, it incorporates a novel selection of genes that have shown significant associations with HCC outcomes, as identified through rigorous bioinformatics analysis. Secondly, our model is underpinned by a comprehensive analytical framework that includes WGCNA, PPI network analysis, and survival analysis, providing a more holistic understanding of the prognostic landscape. Thirdly, our preliminary findings suggest that this model may enhance the accuracy of survival predictions, which is currently under further statistical scrutiny. Additionally, the genes in our model are aligned with the current biological understanding of HCC and may have therapeutic implications, thus offering clinical utility beyond prognosis. Additionally, patients with HCC who have low MSH2 expression have a bad prognosis [27]. Overall, the enriched pathways and terms in the HCC turquoise module give insightful information on the molecular pathways underlying the genesis and progression of diseases. Further research on these pathways may help identify potential targets for new therapies in HCC. The integration of our 26-gene risk model with these pathways could provide a more precise and personalized approach to HCC management and treatment.

Based on the above results and a series of bioinformatics analyses, the key gene *PAK1IP1* was determined in this study. PAK1IP1 is a protein closely related to PAK1 and plays a key regulatory role in various biological processes [28]. P21 (RAC1) activated kinase 1 (PAK1) is a serine/threonine protein kinase belonging to the PAK family, and its abnormal activation is closely related to the development of various tumors. A study has shown that the activation of *PAK1* promotes the proliferation, migration, and invasion of liver cancer cells, as well as the formation of breast cancer stem cells, revealing its essential role in tumor development [29]. Aberrant expression of *PAK1IP1* has been implicated in human diseases [30]. PAK1IP1 interacts with β-catenin and facilitates its nuclear translocation, activating Wnt target genes [31]. Similarly, *PAK1IP1* enhances cell invasiveness in gastric cancer by regulating actin cytoskeleton dynamics [32]. Furthermore, *PAK1IP1* has been implicated in cancer cell survival and chemotherapy resistance [33]. In ovarian cancer, *PAK1IP1* promotes cell survival under hypoxic conditions by regulating the AMP-activated protein kinase (AMPK) signaling pathway. PAK1IP1 binds to and inhibits the activity of AMPK, thereby reducing cell death and promoting cell survival [28]. Our research found that HCC tumor tissue samples had a high expression of *PAK1IP1*. Moreover, clinical tissue samples from liver cancer patients exhibited upregulated expression of *PAK1IP1*. According to the Kaplan-Meier survival analysis, the *PAK1IP1* high-expression group had a poorer OS

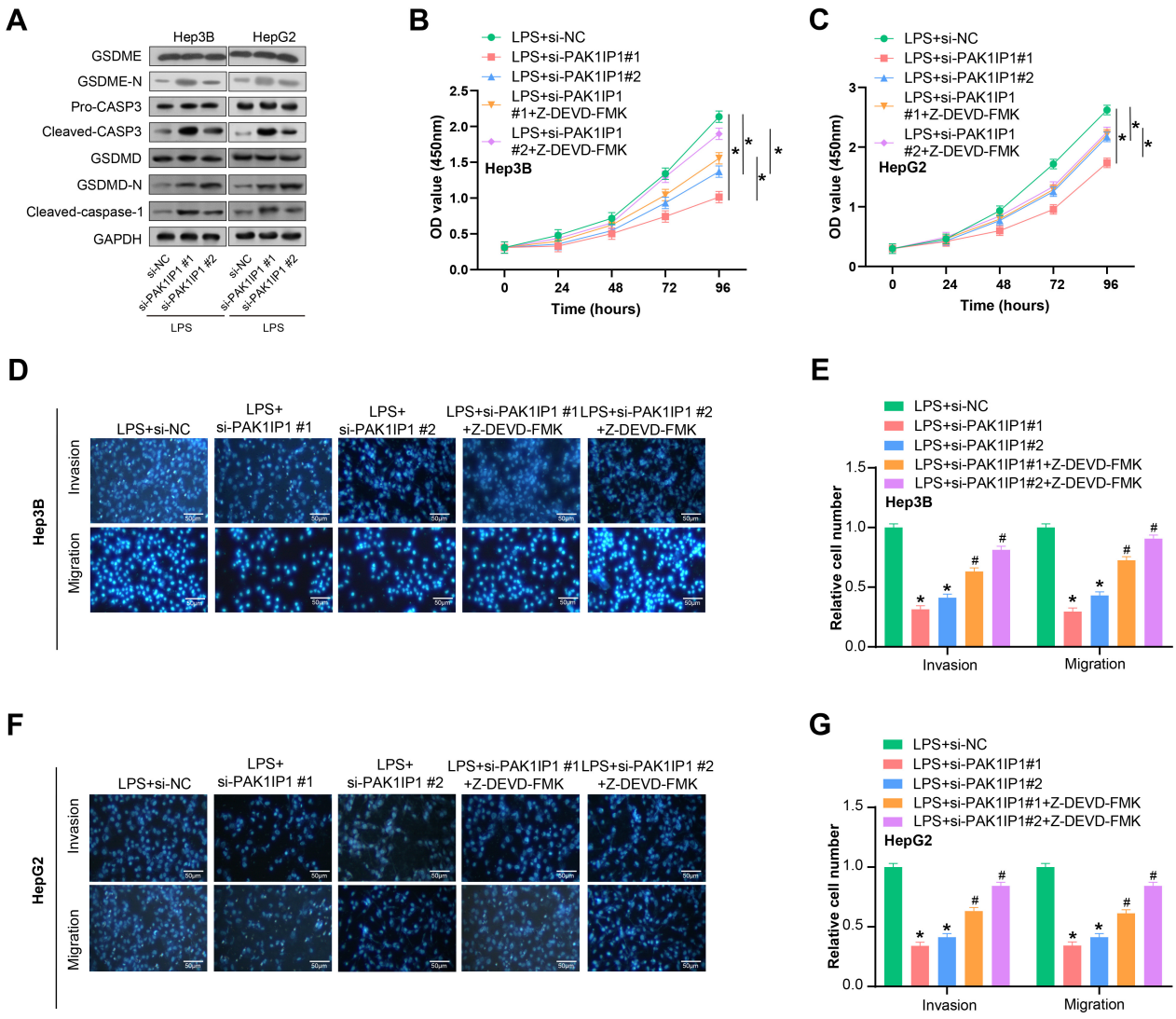

Fig. 9. *PAK1IP1* knockdown suppresses proliferation, invasion and migration of HCC cells through the CASP-3 pathway. (A) WB analysis of caspase 3 (CASP-3), gasdermin E (GSDME)-N, cleaved caspase-1, and gasdermin-D (GSDMD)-N protein expression in HCC cells after *PAK1IP1* knockdown. (B,C) CCK-8 assay showing the effect of si-*PAK1IP1* knockdown and N-benzyloxycarbonyl-Asp (OMe)-Glu (OMe)-Val-Asp (OMe)-fluoromethyl-ketone (Z-DEVD-FMK) treatment on the proliferation of HCC cells. (D,E) Transwell assay showing the effect of *PAK1IP1* knockdown on the invasion and migration of HCC cells after LPS treatment. Scale: 50 µm. (F,G) Transwell analysis showing the effect of Z-DEVD-FMK treatment on the invasion and migration of HCC cells. Scale: 50 µm. *$p <$ 0.05. #$p < 0.05$ vs. si-*PAK1IP1*#1/2. HCC, hepatocellular carcinoma; WB, western blot; CCK-8, cell counting kit-8.

rate than the low-expression group. Overall, *PAK1IP1* acts as a proto-oncogene in liver cancer patients, and its overexpression adversely affects patient outcomes. Understanding the molecular processes that underlie *PAK1IP1*-mediated cancer growth may offer fresh perspectives for creating fresh treatment approaches.

Myeloid dendritic cells (mDCs) have been identified as crucial players in the immune response against cancer [34]. Herein, we found a significant increase in mDC infiltration in HCC patients. These mDCs function as antigen-presenting cells, initiating the activation of T cells to recognize and eliminate cancer cells [35]. Additionally, they contribute to the activation of natural killer (NK) cells, which are essential for tumor surveillance [36]. Moreover, mDCs can generate cytokines that facilitate the recruitment and activation of other immune cells like macrophages and neutrophils, further bolstering the antitumor immune response [37]. In liver cancer, mDCs have been found to be a critical part of initiating and enhancing antitumor immune responses [38]. Notably, mDCs promote the differentiation and activation of CD8+ T cells, which are instrumental in eliminating tumor cells [39]. Furthermore, mDCs produce interleukin 12 (IL-12), which augments the antitumor activity of NK cells [40]. Targeting mDCs has shown promising outcomes in preclinical studies and clinical trials, either as a standalone treatment or in combination with other anticancer therapies. By understanding the role of *PAK1IP1* in mDCs infiltration, we can potentially develop strategies to

modulate mDCs activity, thereby enhancing the effectiveness of immunotherapies. For instance, the tandem action of CD39 and CD73 ectonucleotidases expressed on mDCs can convert ATP to adenosine, which is an important mediator of immunosuppression in the tumor microenvironment (TME) [41]. Targeting these enzymes could reduce the immunosuppressive effects of mDCs and improve the TME, thus enhancing the efficacy of immunotherapies. Additionally, myeloid cell receptor tyrosine kinases (RTKs) such as TYRO3 protein tyrosine kinase (TYRO3), AXL receptor tyrosine kinase (AXL), and MER proto-oncogene, tyrosine kinase (MERTK), and their ligands, have been shown to suppress immune responses, and their inhibition can reduce the immune suppression function of mDCs, increase CD8+ T cell infiltration, and enhance the treatment efficacy of anti-Programmed Cell Death Protein 1 (PD-1) therapy on melanoma [42]. These findings suggest that targeting mDCs and their associated immunosuppressive factors could be a promising approach to improve immunotherapy outcomes. However, it should be noted that the role of mDCs in tumor growth promotion and immune evasion has also been reported in certain types of cancer, necessitating further investigations to comprehend their intricate and multifaceted functions in cancer biology fully. In conclusion, our study underscores the potential significance of mDCs in liver cancer and indicates targeting mDCs could be a promising method to enhance antitumor immune responses. Subsequent studies are imperative to unravel the mechanisms underlying mDC function in cancer and to develop novel immunotherapeutic approaches aimed at harnessing the potential of these cells.

Furthermore, we performed experiments to elucidate the mechanism by which *PAK1IP1* and pyroptosis-related genes contribute to liver cancer. To assess pyroptosis, we utilized ELISA to measure the production of IL-1β, a key pyroptosis marker, in HCC cells following LPS treatment and *PAK1IP1* knockdown. Remarkably, *PAK1IP1* knockdown resulted in a significant upregulation of IL-1β expression in HCC cells. Additionally, WB revealed a significant upregulation of CASP-3, GSDME-N, cleaved caspase-1, and GSDMD-N in response to *PAK1IP1* inhibition. In the process of pyroptosis, CASP-3, GSDME-N, cleaved caspase-1, and GSDMD-N together form a complex regulatory network. CASP-3, as a key executor of caspase, is involved not only in apoptosis but also in triggering pyroptosis by activating GSDME-N, leading to cell membrane perforation. Meanwhile, cleaved caspase-1, as a marker of inflammasome activation, directly participates in the cleavage of GSDMD-N, promoting pyroptosis and the release of inflammatory cytokine IL-1β. The activation and interaction of these proteins jointly advance the process of pyroptosis, triggering a strong inflammatory response and immune surveillance, thereby playing a crucial role in tumor biology and immune responses. Subsequent experiments involved si-*PAK1IP1* knockdown and treatment with Z-DEVD-FMK, a CASP-3 inhibitor, to evaluate the influence on the proliferation, invasion, and migration of HCC cells. Notably, *PAK1IP1* knockdown inhibited the activities of LPS-treated HCC cells, while Z-DEVD-FMK treatment promoted these cellular processes. Our experimental results suggest that *PAK1IP1* may regulate the level of pyroptosis-related genes via CASP-3-dependent pyroptosis. Although previous studies have focused on some known biomarkers in liver cancer, such as GPC3 and AKR1B10, our research, through large-scale data analysis, has provided a broader list of genes that may play a significant role in the pathogenesis of liver cancer. Our study not only confirms some of the known biomarkers but also identifies new potential prognostic genes, which could offer new targets for the diagnosis and treatment of liver cancer.

In this study, we have hypothesized a novel role for *PAK1IP1* in HCC and explored its correlation with prognosis and immune cell infiltration. However, it is imperative to acknowledge the limitations inherent in our research. First, although we validated the function of *PAK1IP1* through qRT-PCR, WB, and a suite of cellular experiments, these experiments were mainly limited to cell lines. We have not yet assessed the relevance of these findings in the *in vivo* tumor microenvironment, which may limit the clinical applicability of our conclusions. Second, while our bioinformatics analysis suggests that PAK1IP1 expression may be related to immune cell infiltration in HCC, we have not yet experimentally validated this relationship. Furthermore, although our study proposed a risk model containing 26 prognostic genes, external validation in an independent dataset is needed to assess the generalizability and reliability of the model. Regarding functional enrichment analysis and pathway identification, we recognized that only limited experimental validation has been performed on the turquoise module. Moreover, biological experiments have a certain degree of inherent variability, which can influence various factors, such as cell passage number, batch-to-batch differences in reagents, and minor variations in experimental conditions. Future research will necessitate a more comprehensive experimental validation of the functional roles of these genes in cancer biology. When considering future research directions, a broader range of *in vivo* studies, including other markers of pyroptosis, repeated experimental validations, and external validation of our prognostic models, will be valuable next steps. Moreover, an in-depth investigation of the immune infiltration and broader roles of *PAK1IP1* in hepatocellular carcinoma biology is crucial. This study reveals the potential significant roles of *PAK1IP1* and other factors in the progression of hepatocellular carcinoma and patient prognosis. However, further experimental and clinical research is required to deepen our understanding and confirm these preliminary findings.

5. Conclusion

To sum up, *PAK1IP1* has been identified as an oncogenic driver in HCC. The increased infiltration of myeloid

dendritic cells in HCC samples highlights their potential as therapeutic immunological targets. Furthermore, our *in vitro* experiments elucidated the mechanism of *PAK1IP1*, revealing that *PAK1IP1* knockdown induced pyroptosis in HCC cells to inhibit HCC progression. These findings laid the groundwork for future research endeavors to develop new clinical biomarkers.

Availability of Data and Materials

The datasets used and/or analyzed during the current study are available from the corresponding author on reasonable request.

Author Contributions

Conception and design of the study, or acquisition of data, or analysis and interpretation of data: XL, ZL, HZ and JC. Drafting the article or revising it critically for important intellectual content: JC, XL, ZL and HZ. Final approval of the version to be submitted: ZL and XL. All authors contributed to editorial changes in the manuscript. All authors read and approved the final manuscript. All authors have participated sufficiently in the work and agreed to be accountable for all aspects of the work.

Ethics Approval and Consent to Participate

Not applicable.

Acknowledgment

We express our deepest gratitude to all those who have made this study possible. Our heartfelt thanks go to the team members for their collaboration and diligent work, and to them who provided insight and expertise that greatly assisted the research. All authors have read and confirmed the acknowledgment.

Funding

This project is funded by the Nantong Health Commission General Program (MS2022020).

Conflict of Interest

The authors declare no conflict of interest.

References

[1] Alqahtani A, Khan Z, Alloghbi A, Said Ahmed TS, Ashraf M, Hammouda DM. Hepatocellular Carcinoma: Molecular Mechanisms and Targeted Therapies. Medicina. 2019; 55: 526. https://doi.org/10.3390/medicina55090526.

[2] Konyn P, Ahmed A, Kim D. Current epidemiology in hepatocellular carcinoma. Expert Review of Gastroenterology & Hepatology. 2021; 15: 1295–1307. https://doi.org/10.1080/17474124.2021.1991792.

[3] Suresh D, Srinivas AN, Prashant A, Harikumar KB, Kumar DP. Therapeutic options in hepatocellular carcinoma: a comprehensive review. Clinical and Experimental Medicine. 2023; 23: 1901–1916. https://doi.org/10.1007/s10238-023-01014-3.

[4] Ferenci P, Fried M, Labrecque D, Bruix J, Sherman M, Omata M, *et al*. World Gastroenterology Organisation Guideline. Hepatocellular carcinoma (HCC): a global perspective. Journal of Gastrointestinal and Liver Diseases. 2010; 19: 311–317.

[5] Zhang FP, Huang YP, Luo WX, Deng WY, Liu CQ, Xu LB, *et al*. Construction of a risk score prognosis model based on hepatocellular carcinoma microenvironment. World Journal of Gastroenterology. 2020; 26: 134–153. https://doi.org/10.3748/wjg.v26.i2.134.

[6] Chaiteerakij R, Addissie BD, Roberts LR. Update on biomarkers of hepatocellular carcinoma. Clinical Gastroenterology and Hepatology. 2015; 13: 237–245. https://doi.org/10.1016/j.cgh.2013.10.038.

[7] Kang K, Li N, Gao Y, Wang C, Chen P, Meng X, *et al*. circKatnal1 Enhances Inflammatory Pyroptosis in Sepsis-Induced Liver Injury through the miR-31-5p/GSDMD Axis. Mediators of Inflammation. 2022; 2022: 8950130. https://doi.org/10.1155/2022/8950130.

[8] Zou Z, Zhao M, Yang Y, Xie Y, Li Z, Zhou L, *et al*. The role of pyroptosis in hepatocellular carcinoma. Cellular Oncology. 2023; 46: 811–823. https://doi.org/10.1007/s13402-023-00787-9.

[9] Li Z, Yang Z, Zhu Y, Fu C, Li N, Peng F. Sorcin regulate pyroptosis by interacting with NLRP3 inflammasomes to facilitate the progression of hepatocellular carcinoma. Cell Death & Disease. 2023; 14: 678. https://doi.org/10.1038/s41419-023-06096-1.

[10] Yan J, Zhang J, Wang Y, Liu H, Sun X, Li A, *et al*. Rapidly Inhibiting the Inflammatory Cytokine Storms and Restoring Cellular Homeostasis to Alleviate Sepsis by Blocking Pyroptosis and Mitochondrial Apoptosis Pathways. Advanced Science. 2023; 10: e2207448. https://doi.org/10.1002/advs.202207448.

[11] Xia X, Wang X, Cheng Z, Qin W, Lei L, Jiang J, *et al*. The role of pyroptosis in cancer: pro-cancer or pro-"host"? Cell Death & Disease. 2019; 10: 650. https://doi.org/10.1038/s41419-019-1883-8.

[12] Hage C, Hoves S, Strauss L, Bissinger S, Prinz Y, Pöschinger T, *et al*. Sorafenib Induces Pyroptosis in Macrophages and Triggers Natural Killer Cell-Mediated Cytotoxicity Against Hepatocellular Carcinoma. Hepatology. 2019; 70: 1280–1297. https://doi.org/10.1002/hep.30666.

[13] Kiraz Y, Adan A, Kartal Yandim M, Baran Y. Major apoptotic mechanisms and genes involved in apoptosis. Tumour Biology. 2016; 37: 8471–8486. https://doi.org/10.1007/s13277-016-5035-9.

[14] Loftus LV, Amend SR, Pienta KJ. Interplay between Cell Death and Cell Proliferation Reveals New Strategies for Cancer Therapy. International Journal of Molecular Sciences. 2022; 23: 4723. https://doi.org/10.3390/ijms23094723.

[15] Li Z, Shen L, Li Y, Shen L, Li N. Identification of pyroptosis-related gene prognostic signature in head and neck squamous cell carcinoma. Cancer Medicine. 2022; 11: 5129–5144. https://doi.org/10.1002/cam4.4825.

[16] Li MY, Liu LZ, Dong M. Progress on pivotal role and application of exosome in lung cancer carcinogenesis, diagnosis, therapy and prognosis. Molecular Cancer. 2021; 20: 22. https://doi.org/10.1186/s12943-021-01312-y.

[17] Wang CH, Wey KC, Mo LR, Chang KK, Lin RC, Kuo JJ. Current trends and recent advances in diagnosis, therapy, and prevention of hepatocellular carcinoma. Asian Pacific Journal of Cancer Prevention. 2015; 16: 3595–3604. https://doi.org/10.7314/apjcp.2015.16.9.3595.

[18] Kim TH, Kim SY, Tang A, Lee JM. Comparison of international guidelines for noninvasive diagnosis of hepatocellular carcinoma: 2018 update. Clinical and Molecular Hepatology. 2019; 25: 245–263. https://doi.org/10.3350/cmh.2018.0090.

[19] Huang S, Duan S, Wang J, Bao S, Qiu X, Li C, *et al*. Folic-acid-mediated functionalized gold nanocages for targeted delivery of anti-miR-181b in combination of gene therapy and photothermal therapy against hepatocellular carcinoma. Advanced Functional Materials. 2016; 26: 2532–2544.

[20] Cabral LKD, Tiribelli C, Sukowati CHC. Sorafenib Resistance in Hepatocellular Carcinoma: The Relevance of Genetic Heterogeneity. Cancers. 2020; 12: 1576. https://doi.org/10.3390/cancers12061576.

[21] Oakley GG, Patrick SM. Replication protein A: directing traffic at the intersection of replication and repair. Frontiers in Bioscience (Landmark Edition). 2010; 15: 883–900. https://doi.org/10.2741/3652.

[22] Anwar SL, Lehmann U. DNA methylation, microRNAs, and their crosstalk as potential biomarkers in hepatocellular carcinoma. World Journal of Gastroenterology. 2014; 20: 7894–7913. https://doi.org/10.3748/wjg.v20.i24.7894.

[23] Zhu Y, Wang S, Xi X, Zhang M, Liu X, Tang W, *et al*. Integrative analysis of long extracellular RNAs reveals a detection panel of noncoding RNAs for liver cancer. Theranostics. 2021; 11: 181–193. https://doi.org/10.7150/thno.48206.

[24] Wurmbach E, Chen YB, Khitrov G, Zhang W, Roayaie S, Schwartz M, *et al*. Genome-wide molecular profiles of HCV-induced dysplasia and hepatocellular carcinoma. Hepatology. 2007; 45: 938–947. https://doi.org/10.1002/hep.21622.

[25] Luo JP, Wang J, Huang JH. CDKN2A is a prognostic biomarker and correlated with immune infiltrates in hepatocellular carcinoma. Bioscience Reports. 2021; 41: BSR20211103. https://doi.org/10.1042/BSR20211103.

[26] Eso Y, Takai A, Matsumoto T, Inuzuka T, Horie T, Ono K, *et al*. MSH2 Dysregulation Is Triggered by Proinflammatory Cytokine Stimulation and Is Associated with Liver Cancer Development. Cancer Research. 2016; 76: 4383–4393. https://doi.org/10.1158/0008-5472.CAN-15-2926.

[27] Lin Z, Xu SH, Wang HQ, Cai YJ, Ying L, Song M, *et al*. Prognostic value of DNA repair based stratification of hepatocellular carcinoma. Scientific Reports. 2016; 6: 25999. https://doi.org/10.1038/srep25999.

[28] Bai Z, Yao C, Zhu J, Xie Y, Ye XY, Bai R, *et al*. Anti-Tumor Drug Discovery Based on Natural Product β-Elemene: Anti-Tumor Mechanisms and Structural Modification. Molecules. 2021; 26: 1499. https://doi.org/10.3390/molecules26061499.

[29] Lin L, Chang J, Tian Y, Chen J. Computer-aided prediction and molecular mechanism investigation of active components in compound Kushen injection inhibiting p21-activated kinase 1. Sheng Wu Yi Xue Gong Cheng Xue Za Zhi. 2024; 41: 313–320. (In Chinese) https://doi.org/10.7507/1001-5515.202306011.

[30] Ross AP, Mansilla MA, Choe Y, Helminski S, Sturm R, Maute RL, *et al*. A mutation in mouse Pak1ip1 causes orofacial clefting while human PAK1IP1 maps to 6p24 translocation breaking points associated with orofacial clefting. PLoS ONE. 2013; 8: e69333. https://doi.org/10.1371/journal.pone.0069333.

[31] Chen X, Huang C, Li K, Liu J, Zheng Y, Feng Y, *et al*. Recent advances in biosynthesis and pharmacology of β-elemene. Phytochemistry Reviews. 2023; 22: 169–186.

[32] Liu JS, He SC, Zhang ZL, Chen R, Fan L, Qiu GL, *et al*. Anticancer effects of β-elemene in gastric cancer cells and its potential underlying proteins: a proteomic study. Oncology Reports. 2014; 32: 2635–2647. https://doi.org/10.3892/or.2014.3490.

[33] Abu-Izneid T, Rauf A, Shariati MA, Khalil AA, Imran M, Rebezov M, *et al*. Sesquiterpenes and their derivatives-natural anticancer compounds: An update. Pharmacological Research. 2020; 161: 105165. https://doi.org/10.1016/j.phrs.2020.105165.

[34] Schreibelt G, Tel J, Sliepen KHEWJ, Benitez-Ribas D, Figdor CG, Adema GJ, *et al*. Toll-like receptor expression and function in human dendritic cell subsets: implications for dendritic cell-based anti-cancer immunotherapy. Cancer Immunology, Immunotherapy. 2010; 59: 1573–1582. https://doi.org/10.1007/s00262-010-0833-1.

[35] Ueno H, Klechevsky E, Morita R, Aspord C, Cao T, Matsui T, *et al*. Dendritic cell subsets in health and disease. Immunological Reviews. 2007; 219: 118–142. https://doi.org/10.1111/j.1600-065X.2007.00551.x.

[36] Mikulak J, Oriolo F, Zaghi E, Di Vito C, Mavilio D. Natural killer cells in HIV-1 infection and therapy. AIDS (London, England). 2017; 31: 2317–2330. https://doi.org/10.1097/QAD.0000000000001645.

[37] Crooke SN, Ovsyannikova IG, Poland GA, Kennedy RB. Immunosenescence: A systems-level overview of immune cell biology and strategies for improving vaccine responses. Experimental Gerontology. 2019; 124: 110632. https://doi.org/10.1016/j.exger.2019.110632.

[38] Choi YJ, Park SJ, Park YS, Park HS, Yang KM, Heo K. EpCAM peptide-primed dendritic cell vaccination confers significant anti-tumor immunity in hepatocellular carcinoma cells. PLoS ONE. 2018; 13: e0190638. https://doi.org/10.1371/journal.pone.0190638.

[39] Scheffel F, Knuschke T, Otto L, Kollenda S, Sokolova V, Cosmovici C, *et al*. Effective Activation of Human Antigen-Presenting Cells and Cytotoxic $CD8^+$ T Cells by a Calcium Phosphate-Based Nanoparticle Vaccine Delivery System. Vaccines. 2020; 8: 110. https://doi.org/10.3390/vaccines8010110.

[40] Lu H, Dietsch GN, Matthews MAH, Yang Y, Ghanekar S, Inokuma M, *et al*. VTX-2337 is a novel TLR8 agonist that activates NK cells and augments ADCC. Clinical Cancer Research. 2012; 18: 499–509. https://doi.org/10.1158/1078-0432.CCR-11-1625.

[41] Sui H, Dongye S, Liu X, Xu X, Wang L, Jin CQ, *et al*. Immunotherapy of targeting MDSCs in tumor microenvironment. Frontiers in Immunology. 2022; 13: 990463. https://doi.org/10.3389/fimmu.2022.990463.

[42] Li K, Shi H, Zhang B, Ou X, Ma Q, Chen Y, *et al*. Myeloid-derived suppressor cells as immunosuppressive regulators and therapeutic targets in cancer. Signal Transduction and Targeted Therapy. 2021; 6: 362. https://doi.org/10.1038/s41392-021-00670-9.